2020

Monitoring the Biochemical Changes Occuring to Human Keratinocytes Exposed to Solar Radiation by Raman Spectroscopy

Ulises Lopez-Gonzalez
Technological University Dublin

Alan Casey
Technological University Dublin, alan.casey@tudublin.ie

Hugh Byrne
Technological University Dublin, hugh.byrne@tudublin.ie

Recommended Citation

Lopez-Gonzalez, U., Casey, A., Byrne, H. (2020). Monitoring the biochemical changes occurring to human keratinocytes exposed to solar radiation by Raman spectroscopy. *Journal of Biophotonics*, October 24, e2020000337. doi:10.1002/jbio.202000337

Received ; | Revised ; | Accepted

DOI: xxx/xxxx

FULL ARTICLE

Monitoring the biochemical changes occurring to human keratinocytes exposed to solar radiation by Raman spectroscopy. †

U. Lopez-Gonzalez*[1] | A. Casey[1] | H. J. Byrne[2]

[1]School of Physics, Nanolab Research Center, FOCAS Research Institute, Technological University Dublin, Dublin, Ireland

[2]FOCAS Research Institute, Technological University Dublin, Dublin, Ireland

Correspondence
*Ulises Lopez Gonzalez, FOCAS Research Institute, Technological University Dublin, Kevin Street, Dublin 8, Ireland. Email: uli.lg27@gmail.com

Present Address
FOCAS Research Institute, Technological University Dublin, Kevin Street, Dublin 8, Ireland

Solar radiation exposure is recognised to be a significant contributor to the development of skin cancer. Monitoring the simultaneous and consecutive mechanisms of interaction could provide a greater understanding of the process of photocarcinogenesis. This work presents an analysis of the biochemical and morphological changes occurring to immortalised human epithelial keratinocyte (HaCaT) cell cultures exposed to simulated solar radiation (SSR). Cell viability was monitored with the aid of the Alamar Blue assay (AB), morphological examination was done with Hematoxylin and Eosin staining (H&E) and changes to the biochemical constituents (nucleic acids and proteins) as a result of the radiation insult were demonstrated through a combination of Raman microspectroscopy and multivariate analysis of spectral patterns. The spectral results suggest that SSR induces changes to the conformational structure of DNA as an immediate result of the radiation, whereas alteration in the protein signature is mostly seen as a later response.

KEYWORDS:
Raman spectroscopy, solar radiation, Principal Component Analysis, Partial Least Squares Regression

Abbreviations: SSR, simulated solar radiation; AB, Alamar blue; H&E, Hematoxylin and Eosin staining; RS, Raman spectroscopy; PCA, Principal Component Analysis; PLSR, Partial Least Squares Regression

1 | INTRODUCTION

Solar radiation is a fundamental factor for life on earth, but also the most effective carcinogenic agent.[1] The composition of the solar spectrum ranges from radiowaves through infrared (IR) further divided into IR-A ($\lambda = 780 - 1400nm$), IR-B ($\lambda = 1400 - 3000nm$), and IR-C ($\lambda = 1mm - 3000nm$), to visible light ($\lambda = 400 - 780nm$) and ultraviolet (UVR) composed of UV-C (wavelength; $\lambda = 100 - 280nm$), UV-B ($\lambda = 280 - 315nm$), and UV-A ($\lambda = 315 - 400nm$).[2] Significant attention is focused on the UV region of the solar spectrum,[3–6] since it is the initiator of multiple biochemical events in skin cells, such as generation of free radicals, alteration in the structure of DNA and proteins, chronic depression of key physiological processes and physiological stress, resulting in reduction of cell growth and cell division.[6,7] Additionally, IR radiation can induce premature skin aging through stimuli of vessel formation, inflammatory cells recruitment and oxidative DNA damage,[8] whereas visible light has been implicated in erythema, pigmentation and radical production.[9] Excessive and recurrent exposure to solar radiation can greatly generate adverse health effects, including skin cancer, cutaneous malignant melanoma, non melanoma basal cell carcinoma and squamous cell carcinoma.[10,11] The metabolic cell response to solar radiation insult can occur acutely and in a delayed manner.[4] Inflammatory response, originating from a cascade of cytokines, vasoactive and neuroactive mediators and DNA single and double strand breaks are strongly associated with direct effects of UVR on skin,[4,10] whereas

†Monitoring the biochemical and morphological changes occurring to human keratinocytes exposed to solar radiation by Raman spectroscopy

generation of reactive oxygen species (ROS), protein modifications and oxidation, and energy depletion are some of the later responses to solar radiation.[11,12] Histological techniques such as routine Hematoxylin and Eosin staining (H&E),[13] immunohistochemistry (ICH),[14] and the more sophisticated in situ hybridisation techniques[15] are commonly used in medical diagnosis of skin neoplasms. These techniques can highlight morphological changes to the cellular architecture, subcellular spatial distribution and show a wide range of normal and abnormal cell and tissue components.[11–14,16,17] Such techniques do not, however, monitor or provide insight into biochemical changes at a tissue/cellular level, or differentiate the initial, direct photochemical changes and the subsequent metabolic perturbations induced by sunlight. In this context, Raman spectroscopy offers an alternative to study the interaction mechanisms between solar radiation and the molecular species and structures within the tissue and individual cell.[3,11] This technique has been employed successfully for diagnosis of metabolic disorders, cell death mutagenesis, carcinogenesis processes, among others.[11,18–21] As a label free, optical microspectroscopic technique, it offers several advantages such as high spatial resolution ($\sim 0.5\mu m$ to $1.5\mu m$) which allows spectral measurements at the subcellular level (e.g. nuclei, cytoplasm).[19,22] Experiments in aqueous media can also be performed since water has a relatively weak contribution, compared to IR absorption spectroscopy, enabling studies with cells alive in normal physiological conditions.[19,23] The present work aims to highlight the potential of Raman spectroscopy coupled with multivariate analysis for the detection and analysis of direct photobiological effects and the later impact of the solar radiation on the cell metabolism. As an initial exploration of the techniques, the responses of in vitro keratinocyte cell cultures are monitored, immediately after exposure solar irradiation, and 24hrs post irradiation. Multiple environmental factors such as weather conditions, time of day, geographical location, to name but a few, can influence the natural solar irradiance.[2] Therefore, in this study, an artificial source of full spectrum, simulated solar irradiation was used to maximise reproducibility, stability and reliability of the data.

1.1 | Materials

Cell culture media, foetal bovine serum, L-glutamine and trypsin were purchased from Sigma Aldrich Ltd (Arklow, Co. Wicklow, Ireland). Alamar Blue® (AB) was purchased from Biosciences (Dublin, Ireland). Cell culture media (phenol red - free) were purchased from Thermo Fisher Scientific.

1.2 | Cell culture

HaCaT, immortalised human dermal keratinocyte cells, were purchased from the Leibnitz Institute DSMZ, German Collection of Microorganisms and Cell Cultures. Cells were cultured in Dulbecco's Modified Eagle Medium: Nutrient Mixture F-12 (DMEM/F12) supplemented with 10% foetal bovine serum, and 1% L-glutamine in a humidified atmosphere containing 5% CO_2 at $37°C$.[24] Cells were cultured until they reached approximately 80-90% confluency. Cells were detached by trypsin and seeded at a concentration of 1×10^5 cells per well in 6 well plates for the AB assays, onto sterilised, circular calcium fluoride (CaF_2) windows (Crystan, UK) immersed in Petri dishes (30 mm diameter, Stardust, USA) for Raman spectroscopic measurements and on glass cover slips immersed in Petri dishes for fixed cell, light microscopy imaging.[25] All samples were incubated for 24 h prior to irradiation, to allow cell attachment.

1.3 | Dosimetry

A Q-sun solar simulator (Q-panel, Cleveland, USA) was employed to irradiate the samples to explore the effects of solar damage to cells. This simulator provides irradiance over the entire solar spectrum, including the UVA and UVB regions.[26] The light from the lamp is modified by internal optical filters to ensure the required spectrum (almost identical to Noon Summer Sunlight at the equator), and desired intensity of irradiance of the light at the sample is specified by the user, and controlled by sensors inside the Q-sun. Integrating the spectral distribution from 280nm-400nm yielded a total UV intensity of $63.63 W m^{-2}$, $62.30 W m^{-2}$ in the UVA (315-400 nm) and $1.33 W m^{-2}$ in the UVB (280-315 nm) region.[26] The Q-sun simulator is calibrated every 1000 hrs. In the results section, exposures are quoted in terms of exposures time. However, they can be converted to UV dose, noting that $1 W m^{-2}$ equals $1 J m^{-2} s^{-1}$. For instance, a 30 min (1800 s) exposure with an irradiator providing UV irradiance of $63.60 W m^{-2}$ ($63.60 J m^{-2} s^{-1}$) provides a dose of $114,480 (63.60 \times 1800) J m^{-2}$ or $11.45 J cm^{-2}$.

1.4 | Solar exposure

Prior to exposure to simulated solar radiation (SSR), the culture medium in the samples was removed and exchanged for phosphate buffered saline (PBS), thus avoiding cell death due to the formation of reactive oxygen species (ROS) via riboflavin photosensitisation and degradation present in the cell culture medium, as observed in previous studies.[11,27] The irradiation compartment of the Q-sun was sterilised with 100% methanol in order to perform the irradiation experiment without plastic lids, thus ensuring the samples are exposed

to the full simulated solar spectrum. Previous studies have demonstrated that little or no differences in cell viability were exhibited by controls maintained in the incubator, or removed and "sham irradiated" in the solar simulator,[27] and therefore control samples were treated in the same manner as the irradiated ones, with the exception of the irradiation exposure time while they were kept in the incubator. After ignition, the Q-sun was allowed to stabilise for 15 min. The temperature of the chamber is stabilised to $37°C$. Exposed samples were irradiated for 30, 60, 90, 120 and 180 min. Post exposure, samples were removed from the compartment of irradiation and divided into two groups. Group one was used for cell viability assessment, Raman spectroscopy measurements or microscopy image acquisitions, immediately (taking into account sample preparation, approx. 10 min) after irradiation. From group two, the PBS was removed and replaced by pre-warmed medium, and samples were returned to the incubator at 5% CO_2 at $37°C$ before their further analysis, 24 hr post-exposure.

1.5 | Light microscopy imaging

Samples were processed for morphological examination immediately after irradiation (within 10 min for sample preparation) and 24 h post exposure by using hematoxylin and eosin staining (H&E).[28] All samples were cover slipped and observed under a light microscope (Olympus BX51) at 100× magnification (Olympus MPLN, NA 0.9) and photographed.

1.6 | Cell viability measurement with Alamar Blue

Due to its non-toxic properties and sensitivity, the AB assay has become one of the most referenced methods to assess metabolic function and cellular health in research as well as in irradiation studies.[29–31] In the AB assay, the blue, non-fluorescent and cell membrane permeating reagent (Resazurin) is reduced to its pink highly fluorescent state (Resorufin), as an indicator of the metabolic activity of cells.[30] Thus, in this study, the AB reduction can serve as an indication of the presence of live cells in the biological system after exposure to UV/solar radiation. Cell viability was determined by AB for both experiments, immediately after irradiation (within 10 min for sample preparation) and 24 h incubation post-exposure. The experiment was performed in triplicates, dividing each plate into three parts and considering one 6-well plate per time point. Cells were seeded to a density of 1×10^5 cells per well. Untreated plates exposed to medium with no irradiation were also included in the experimental design as control. Post irradiation exposure, PBS was removed and samples were incubated in 3 ml of AB solution (5% [v/v] solution of AB dye) prepared in pre-warmed, un-supplemented (no FBS) medium and incubated for 3 h at $37°C$, 5% CO_2. AB conversion, as a measure of the metabolic activity of cells, was determined by using a plate reading spectrometer (SpectraMax—M3) to monitor fluorescence with 540 nm excitation and 590 nm emission.

1.7 | Raman Spectroscopy

A Horiba Jobin-Yvon LabRAM HR800 spectrometer with an external 300 mW diode laser operating at 785 nm as source was employed in this work. The power on the sample was ∼ 70 mW. A 100× (Olympus LMPLFLNx100, NA 0.8) immersion objective was used for the measurements, providing a spatial resolution of $\sim 1\mu m$ at the sample. The water immersion environment acts as a heat sink, reducing the risk of photothermal damage of the cells.[32] As part of the confocal operating settings, the confocal hole was set at 100 μm. The system was spectrally calibrated to the 520 cm^{-1} line of silicon, and the intensity response function was corrected using the Standard Reference Material (SRM) No. 2243 of the national Institute of Standards, Boulder, Colorado, USA (NIST SRM 2243, 2242, 2241).[33] The LabRAM system is a confocal spectrometer that contains two interchangeable gratings (300 and 900 lines per mm respectively). In this experiment, the 300 lines/mm grating was used, providing a spectral dispersion of approximately 1.5 cm^{-1} per pixel, resulting in a full width half maximum of the source 785 nm laser line of 6.16 cm^{-1}. The lower dispersion grating enables the spectral range of the fingerprint region, from 400 cm^{-1} to 1800 cm^{-1}, to be captured in a single spectral window. The detector used was a 16-bit dynamic range Peltier cooled CCD detector. For Raman spectroscopic analysis, the HaCaT cells were seeded onto sterilised calcium fluoride (CaF_2) circular windows immersed in Petri dishes (30 mm diameter) at a density of $1x10^5$ in a volume of 200 µm of 10% FBS DMEM/F12. The cells were then incubated for 1 h to encourage the cells to attach on the (CaF_2), after which 3 ml 10% FBS DMEM/F12 were added. After 24 h incubation with 5% CO_2 at $37°C$, cells were irradiated, as outlined in Section 1.4. The experiment was performed in triplicates, whereby each irradiation time point (30, 60, 90, 120 and 180 min) is represented by three individual Petri dish plates, as well as three control plates. Raman spectroscopic analysis was undertaken both immediately (within 2 min for sample preparation per sample) after irradiation and 24 h incubation post-exposure. After exposure in the Q-sun, the PBS in the samples was changed for pre-warmed DMEM/F12 (phenol red free) medium for the Raman spectroscopic analysis. Ten keratinocyte cells from each Petri dish plate were selected to acquire single Raman spectra, focusing on their nucleus to

specifically explore DNA damage after simulated solar radiation exposure. The backscattered Raman signal was integrated for 30 s and accumulated two times to improve signal-to-noise ratio, and 30 spectra for control and irradiated samples were collected to perform pre-processing methods (baseline correction, smoothing and normalisation) to further improve the quality of the acquired spectra for their analysis. A number of other studies have used similar methodologies[34–36] demonstrating that the variability across the cell population is less than between populations which have undergone treatment with exogenous agents, enabling identification of significant changes as a result of treatment.

1.8 | Data analysis

For AB, three independent experiments were conducted for each time point. Test results for each time point were expressed as percentage of the control +/- standard deviation (SD). Control values were set as 100%. Raman spectra were pre-processed and analysed using Matlab 2017 (Mathworks, USA) to remove the background signal and facilitate an accurate comparison of cell spectra. Extended Multivariate Signal Correction (EMSC) is a model-based multivariate data pre-processing method, based on linear statistical regression modelling.[37] The EMSC method has been previously employed for baseline correction and background signal removal.[22,38] In this work, this approach is used to remove the background signal originating from the water in the un-supplemented DMEM/F12 (phenol red free) medium used in the Raman measurements. This water contribution, whose OH bending vibration appears at 1640 cm^{-1}, overlaps with features of proteins in the Amide I region, potentially interfering with the spectral interpretation. The EMSC algorithm adapted from Kerr et al.[38] and used in this work, can be presented as follows: The raw spectrum, S, consists of Raman spectrum of interest, R, a baseline signal, B, and the water signal, W.

$$S = R + B + W \tag{1}$$

The Raman spectrum, R, can be described by a reference spectrum, r, which can be the average spectrum of the sample data multiplied by a certain scalar weight, Cr.

$$R \sim C_r \times r \tag{2}$$

Similarly, the water signal, W, is described by an average spectrum, w, recorded directly from CaF_2 immersed in DMEM/F12 medium and multiplied by a certain scalar weight, Cw.

$$B = \left[C_w \times w\right] \tag{3}$$

The slowly varying baseline, B, can be represented using an appropriate N order polynomial expressed in eq. 4

$$B_N = C_0 + C_1 \times X + C_2 \times X^2 + C_N \times X^N \tag{4}$$

where N is the order of the polynomial, and Cm for $m = 0 \rightarrow N$ represents the various coefficients in the polynomial. The EMSC algorithm will generate estimates values for the scalar weights Cr, Cw and Cm. These estimates are based on an optimal fit of the various vectors

$$S \sim \left[C_r \times r\right] + \left[C_w \times w\right] + \left[\sum_{m=0}^{N} C_m X^m\right] \tag{5}$$

The background corrected cell spectrum, T, is given by

$$T = \frac{S - \left[C_w \times w\right] - \left[\sum_{m=0}^{N} \times C_m X^m\right]}{C_r} \tag{6}$$

In this paper, the reference spectrum is the mean spectrum of 30 HaCaT cell nuclei spectra, acquired on CaF_2 disc. The selected polynomial order was N=5, correcting the baseline and removing the water contribution from the spectra. Subsequently, the corrected spectra were smoothed using the Savitzky–Golay method (polynomial order of 5 and window 13) and vector normalised to improve spectral quality and minimise the possible influences of measurement variability. Principal components analysis (PCA) and partial least squares regression (PLSR), combined with 10-fold cross-validation, were used as multivariate approaches to analyse the Raman spectra. PCA reduces the number of variables in a multidimensional data set (i.e. spectra).[11] The extensively applied PLSR technique is a linear model that associates variations in the spectral data to a series of targets.[22,39] The targets used in this work are time of irradiation (e.g. 30 min, 60 min, 90 min, 120 min and 180 min) and AB assay response (% cell viability). 10-fold cross validation approach was used to validate the predictive model.[40] The goodness of fit R^2 (correlation between cell damage and spectral data) value and the mean squared error of prediction (MSEP) obtained from the 10 fold in cross validation were used to evaluate the performance of the regression model and select the optimal number of latent variables. The MSEP plots are shown in the Supplementary Material. In this work, the PCA scores plot is used to visualise whether the spectra coming from cells irradiated at different time points are differentiated, while the PC loadings provide information regarding the biochemical origin of the variability inside the data. Although the PLSR technique can be used to build prediction models based on the spectroscopic responses,[22,39] in this work, the regression co-efficients were used to identify the direct effects of radiation on the cell nuclei as a function of (i) radiation exposure time and (ii) the toxicological response as measured by the AB assay.One-way ANOVA was performed on PC scores to verify the significance of group differences. A P value less than 0.05 was considered statistically significant.

2 | RESULTS

2.1 | Light microscopy imaging

Visualisation of HaCaT cells before and after SSR exposure by light microscopy aims to elucidate the impact at a cellular level. In this study, hematoxylin and eosin (H&E) stains, which are frequently used for histologic examination,[41] were employed to reveal the morphology of cells. The basic dye hematoxylin has an affinity for negatively charged molecules such as DNA and RNA, and thus it is used to reveal the location of the nucleus. The acidic dye eosin binds to positive charged molecules within the cytoplasm.[28] Figure 1 shows a series of images illustrating the progression from control (non-irradiated cells) to highly damaged irradiated HaCaT cells. Both column A and B display successive images, representing different times of exposure to simulated solar radiation. However, column A presents images of cells stained immediately after irradiation, while column B shows images of cells stained 24 hrs post exposure. In general, control cell images show large nuclei with dark-blue nucleoli and some cells in the mitotic phase. As the irradiation time increases, morphological and structural changes can be observed in both columns of images. In column A, even though the changes seen from 30 to 120 min of exposure are not very dramatic, there are some common features, such as chromatic clumping or nuclear fragmentation. Mitotic cells, as in the control, are no longer evident and the appearance of some giant cells (red arrows) can be observed at all radiation times. Cells imaged after 180 min of exposure are seen to be the most damaged of all exposure times, as evidenced in column A by loss of cytoplasmic membrane and chromatin condensation. In column B, the radiation damage is more evident, from the first irradiation time point. The image corresponding to 30 min after exposure shows enlargement of cells and the presence of apoptotic bodies. Cells exposed for in excess of 60 min show common features, such as cytoplasmic degeneration and chromatin condensation, revealing the damage induced by the SSR.

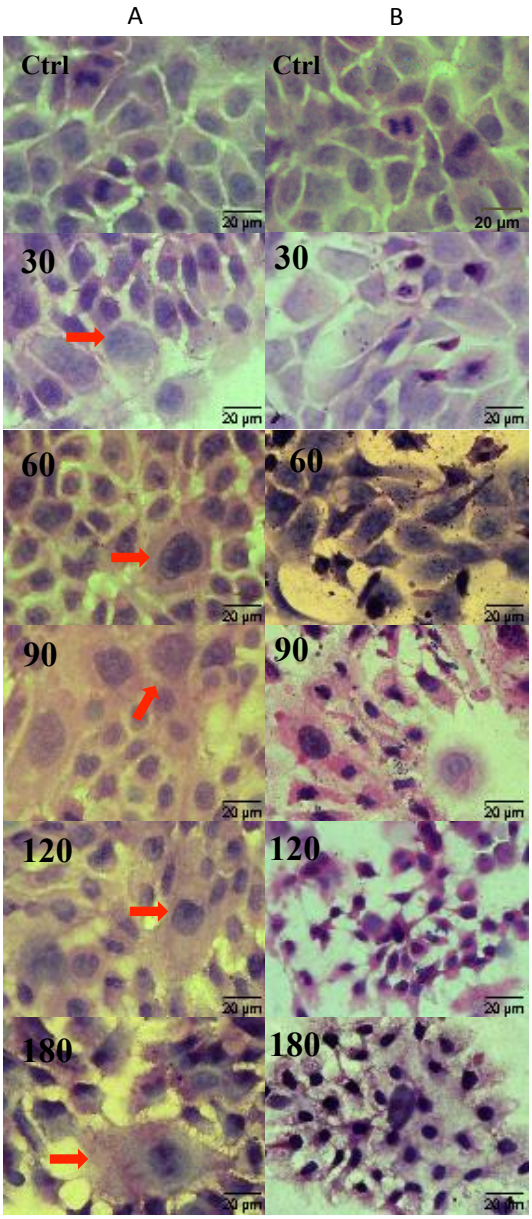

FIGURE 1 Microscopic examination of the H&E stained control and exposed samples (30, 60, 90, 120 and 180 min) to simulated solar radiation for both times of analysis A) immediately after irradiation and B) 24 h post exposure.

2.2 | Cell viability measurement with Alamar Blue

A more quantitative assessment of the effects on the cell culture of SSR exposure can be provided by evaluation of the cytotoxic response. The AB assay is a measure of mitochondrial metabolic activity of cells,[29] which can be impacted by exposure to SSR. In this study, the viability of HaCaT cells was examined after SSR exposure for variable times. The results for both analysis time points (immediately and 24hrs post exposure), as determined by the AB assay, are shown in Figure 2. In both analyses, HaCaT cells exhibit a monotonic decrease in AB fluorescence intensity, compared to control, as a result of the radiation. Notably, cells examined after 24 hrs present lower viability levels than cells analysed immediately after the radiation, especially those irradiated for in excess of 60 min, which exhibit a drastic drop in the viability levels below 5%, when compared to control. However, biochemical information concerning the effects of radiation within cells is still lacking.

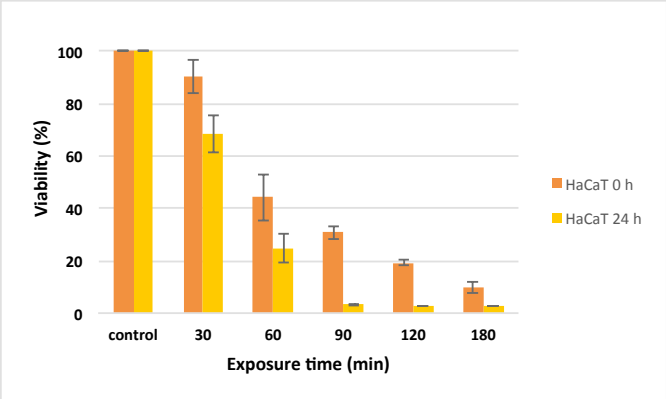

FIGURE 2 Alamar blue response of HaCaT cells (1×10^5 per well) to simulated solar irradiation for varying exposure times, measured immediately and 24 h post exposure.

2.3 | Biochemical characterisation of HaCaT cells on CaF_2 with Raman spectroscopy

Raman spectrometry is a powerful technique for analysing the chemical structure of matter.[42] In the case of biological samples, each of the constituent biomolecules has a unique molecular structure, which provides a distinctive, signature Raman spectrum.[42] Raman spectra of pure biomolecules (i.e. proteins, nucleic acids, lipids, carbohydrates) have been reported previously in several studies.[10,42–44] These biomolecular signatures can be employed to assist in the interpretation of cellular and subcellular spectra[45] (Table 1).

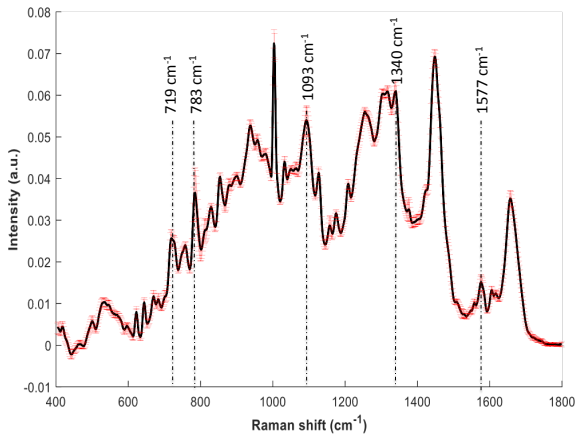

FIGURE 3 Average Raman spectrum of the nuclei of HaCaT cells cultured on a CaF2 disc. The highlighted bands correspond to molecular vibrations originating from nucleic acids within the nucleus of the cells. The red shaded area defines the standard deviation on the mean.

In this work, Raman spectroscopy was employed to provide a spectroscopic characterisation of the HaCaT cell line cultured on CaF_2 to further investigate the biochemical

TABLE 1 Assignments of Raman Bands.[3,19,21,23,44] (A-Adenine, C-Cytosine, G-Guanine, T-Thymine, U- Uracil).

Raman band (cm^{-1})	Assignment
627	G, A
682	G
716-19	A
728	A (ring breathing mode of DNA/RNA bases)
748	T
777	U based ring breathing mode
783	T, C, O-P-O phosphodiester bands in DNA
792-4	C,U,T Nucleobase in DNA and RNA
813	O-P-O, Backbone, DNA
834-6	Amide III, Tyrosine
853	B-DNA
925	Deoxyribose
981	C-C stretching in proteins
1003	phenylalanine, C-C skeletal
1046	Carbohydrates
1062-4	C-N stretching
1091-93	Symmetric PO_2^- stretching vibration of the DNA backbone-phosphate backbone
1121	C-O bond deoxyribose
1132	Deoxyribose-phosphate moiety
1216	Nucleic acids
1230	A
1255	A,T (ring breathing modes of the DNA/RNA bases) amide III
1270	Amide III
1298	A
1323	G
1339-40	Nucleic acid mode
1375-6	T,A,G
1400	CH2
1420-80	G, A (DNA, RNA)
1438	lipids
1460	deoxyribose
1465	lipids
1493	DNA
1577	G
1650-60	C=C (Amide I)
1670-83	Amide I $\beta - sheet$

changes occurring when SSR interacts with cells, at different time points. In Figure 3 is presented the fingerprint region (400 cm^{-1} to 1800 cm^{-1}) of the mean Raman spectrum for HaCaT cells grown on a CaF_2 disc. For illustrative purposes, the highlighted bands correspond to signatures of molecular vibrations originating from nucleic acids within the nucleus of the cells, extensively identified in literature. The spectrum of the nuclear region is also rich in bands associated with proteins and lipids which contribute to the nuclear function.[46,47] Table 1 summarises the spectral peak assignments employed in this work.[3,19,21,23,44] The laser was focused on the nuclear region of the cells, thus, the spectrum contains, among others, characteristic bands of DNA and/or RNA, originating from various moieties like sugar, phosphate, bases, etc. For instance, the bands located at 719 cm^{-1} and 783 cm^{-1} are due to the ring breathing of adenine (A) and O-P-O Backbone, Thymine (T) and Cytosine (C) respectively, while the bands at 1093 cm^{-1}, 1255 cm^{-1}, 1340 cm^{-1} and 1577 cm^{-1} are due to backbone-phosphate backbone vibrations of DNA, and ring modes of T, A, and guanine (G), respectively. Bands associated with proteins are also present in the spectrum, including those at 853 cm^{-1}, 1003 cm^{-1}, 1130 cm^{-1}, and 1650 cm^{-1}.[21,23,44]

PCA was performed to reduce the high-dimensional spectral data to scores on the PCs, thus highlighting the main molecular species responsible for the variation between spectra. Although some degree of clustering is evident in a PCA of all data, no clear trend on which to base a loadings analysis is obvious (Supplemental Figure 5S). Therefore, a binary (pairwise) scores analysis was conducted, which compares control with each time of irradiation, according to the methodology of Bonnier et al.[34] In all cases, PC3 accounted for 10% of the variance and did not contribute to differentiation of the datasets. Initially, the spectra of exposed cells were compared to those of control immediately after irradiation, to elucidate the direct biochemical effects of the radiation. Figure 4 presents scatter plots (a) corresponding to the comparison between control (green) and irradiated (blue) cells, at different exposure times and loading of the second PCs (b), associated to control and 180 min. The spectral acquisition was done immediately after irradiation. Although PC1 (explained variance 46%) accounts for the most variance in the data sets, it does not show significant differentiation of the groups; however, it shows the diversity across the groups, due to point to point intra-sample variability. Among data for different irradiation exposure times, only cells exposed for 180 min show a clear differentiation from control cells. However the separation between these two groups is observed in PC2 (explained variance 14%), whereby control cells predominantly scored negatively and approximately half of the irradiated cells scored positively. No significant statistical differences were found between control and irradiated cells analysed immediately after irradiation (p>0.05), except for cells irradiated for 180 min (p= 6.00×10^{-4}).

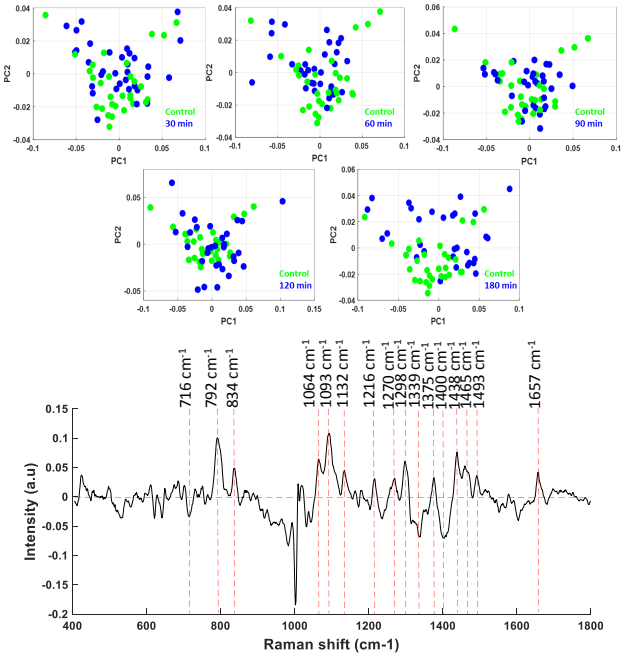

FIGURE 4 PCA scatter plot (a) and loading of PC2 (b), corresponding to comparison of control versus 180 minutes of exposure. The Raman spectral acquisition was done immediately after irradiation. The red vertical dotted lines in the spectra highlights the regions where conformational and biochemical changes are occurring due to the action of SSR in cells while horizontal red dotted line represents the zero point in PC2. No significant differences were found for control vs 30 (p=0.051); 60 (p=0.156); 90 (p=0.986) and 120 (p=0.516), except for ctrl vs 180 (p= 6.00×10^{-4}).

In figure 4(b), the PC2 loadings for 180 min versus control are presente. Positive features of the loading are manifest more strongly in spectra which score positively in the scatter plot, and vice versa for negative features.[34] The PC2 loading is dominated mainly by positive contributions of nucleic acids (792 cm^{-1}, 1093 cm^{-1}, 1132 cm^{-1}, 1216 cm^{-1}, 1298 cm^{-1}, 1375 cm^{-1}, and 1493 cm^{-1}) and proteins (834 cm^{-1}, 1064 cm^{-1}, 1270 cm^{-1} and 1657 cm^{-1}). The prominent bands contributing to the negative loadings are due to proteins (1003 cm^{-1}) and nucleic acids (716 cm^{-1} and 1339 cm^{-1}).

PCA was also carried out to compare spectra recorded from cells immediately after irradiation and 24hrs post exposure. This comparison should elucidate the impact of the irradiation on the cell metabolism, post exposure. Figure 5 shows the corresponding scatter plots (a) and second loading of the PCA (b). PC1 (explained variance 55%), which represent the most significant variance among the data, does not differentiate

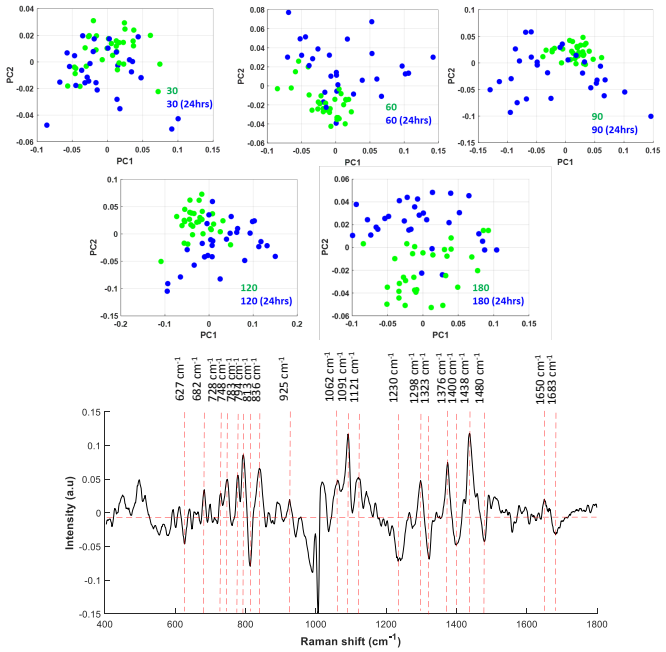

FIGURE 5 PCA scatter plot (a) and loading of PC2 (b), corresponding to comparison of cells exposed for 180 min analysed immediately and 24 hrs post exposure. Red dotted line indicates the zero point in the PC2 loading. The red vertical dotted lines in the spectra highlights the regions where conformational and biochemical changes are occurring due to the action of SSR in cells while horizontal red dotted line represents the zero point in PC2. Significant statistical differences were found between groups: 30 and 30 (24 hrs) p= 3.00×10^{-4} ; 60 vs 60 (24 hrs) p= 4.22×10^{-8}; 90 vs 90 (24 hrs) p= 4.62×10^{-6}; 120 vs 120 (24 hrs) p= 7.26×10^{-6} and 180 vs 180 (24 hrs) p= 3.64×10^{-11}.

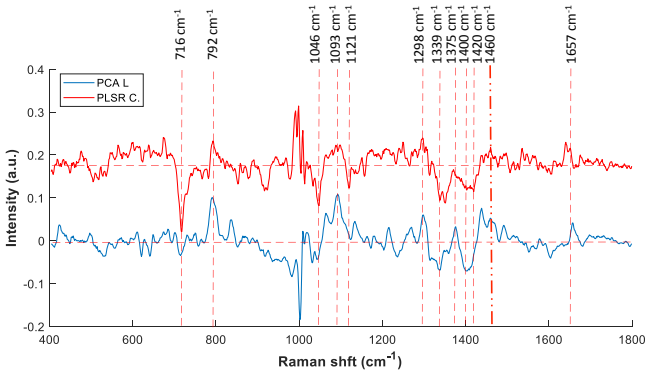

FIGURE 6 PLSR against exposure time for Raman spectra of cells analysed immediately after irradiation, (PLSR C) plot of PLSR coefficient for regression against exposure time and (PCA L) PCA loadings of control vs 180min. The red vertical dotted lines in the spectra highlights the regions where conformational and biochemical changes are occurring due to the action of SSR in cells while horizontal red dotted line represents the zero point in PC2 and PLSR co-efficient.

between the datasets, but highlights the cell-to-cell variability. The spectra for the nucleus of cells analysed immediately after irradiation are mostly clustered together, with the exception of the 180 min time-point, while cells analysed 24 hrs post exposure tend to be more scattered, located on both the negative and positive side of PC1. However, compared to the results of Figure 4, the spectra related to cells analysed 24 hrs post exposure are relatively well differentiated from cells analysed immediately after irradiation according to PC2, with the exception of those cells exposed for only 30 min. The variance between the groups is highlighted by PC2 (explained variance of 20%). The predominant features, which differentiate the spectra of cells analysed immediately and 24 hrs post exposure in the PC loading comparing 180 min (immediate) and 180 min (24 hrs post exposure) are associated with nucleic acids (682 cm^{-1}, 728 cm^{-1}, 748 cm^{-1}, 783 cm^{-1}, 794 cm^{-1}, 925 cm^{-1}, 1091 cm^{-1}, 1121 cm^{-1}, 1298 cm^{-1} and 1376 cm^{-1}) and proteins (836 cm^{-1}, 1650 cm^{-1}). In the negative aspect, associated with cells 24 hrs after irradiation, the dominant features are due to nucleic acids (627 cm^{-1}, 813 cm^{-1}, 1230 cm^{-1}, 1323 cm^{-1} and 1480 cm^{-1}), and proteins (1683 cm^{-1}). (table 1).[19,21,23,44] Notably, the spectral profile of the differentiating PC loading 24 hrs after irradiation is significantly different to that immediately after exposure, indicating the spectroscopic profiles contain information related to the longer term responses of the cell, post irradiation, as well as to the direct impact of irradiation. Statistically significant differences were observed in the comparison of groups of cells analysed immediately and 24 hrs post exposure ($p<0.005$), as determined by ANOVA test.

In order to explore this further, the spectroscopic data was subjected to PLSR using the target of (i) exposure time immediately after irradiation, to identify signatures of direct radiation damage, and (ii) the AB cell viability 24 hrs after irradiation, to identify signatures of cellular response. For (i), the MSEP plot, presented in Figure S2.b of the Supplementary Information, shows that 3 or 4 components can be sufficient to account for 90% of the variance. However, 5 components were selected to fit the model, since it gives a better linear prediction plot than using fewer components. A correlation accuracy (R^2) of 0.91 was obtained for the model, which is illustrated in Figure 4S confirming the linear trend of the regression and the intrasample variability. The PLSR co-efficient plot is displayed in Figure 6, compared with the PC2 loading of Figure 4. Similar to PC loadings[34], PLSR co-efficient can exhibit positive and negative features, which either increase, or decrease as a function of the external target variable.[48] Negative spectral features, associated with decreased contributions

as a function of irradiation time, are mainly due to nucleic acids (716 cm^{-1}, 1121 cm^{-1}, 1339 cm^{-1} and 1420 cm^{-1}) which are also present as negative loadings in the PC2 loading, and characterise control cells. The positive spectral feature in Figure 6 due to O-P-O phosphodiester (792 cm^{-1}, 1093 cm^{-1}) is also present in the PC2 loading as a feature of the spectra of irradiated cells.[19,21,23,44] The spectroscopic data, acquired immediately after exposure, was also regressed against cell viability, although the correlation co-efficient proved to be almost identical to that of the regression against exposure time (albeit inverted) (Figure 3Sa), which is understandable as the viability and time are quite closely (inversely) correlated (Figure 1). The PLSR technique was also applied to the Raman spectra of cells analysed 24 hrs post exposure. The Raman data was regressed against cell viability to elucidate spectral features associated to metabolic changes within cells. Seven components were used to fit the model, (see MSEP plot in Figure S2.b) yielding an R^2 value of 0.91. The PLSR co-efficient plot is shown in Figure 7, along with the PC2 loading of Figure 5. It should be noted that positive PLSR features are those which are associated with decreased cell viability, whereas positive PCA loadings are those which are stronger in the spectra 24hrs post 180 hrs post irradiation, than immediately. The PLSR co-efficient exhibits positive spectral features associated with nucleic acids (783 cm^{-1}, 813 cm^{-1} and 1480 cm^{-1}) and proteins (981 cm^{-1}), which also feature as negative bands of the PC2 loading (also shown in Figure 6), and correspond to spectra of cells analysed immediately after irradiation.

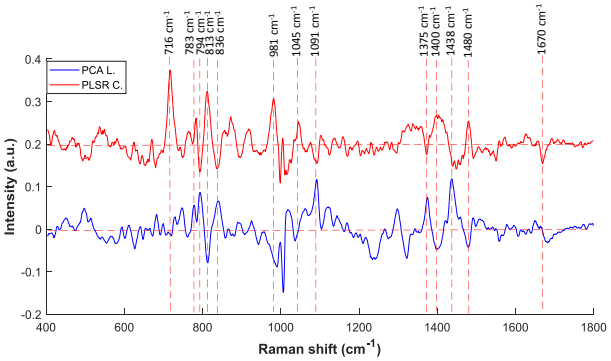

FIGURE 7 PLSR modeling versus cell viability for Raman spectra of cells analysed 24hrs post exposure, (PLSR C) plot of PLSR coefficient for regression against cell viability and (PCA L) PCA loadings of 180 min vs 180 min (24hrs). The red vertical dotted lines in the spectra highlights the regions where conformational and biochemical changes are occurring due to the action of SSR in cells while horizontal red dotted line represents the zero point in PC2 and PLSR co-efficient.

The negative spectral features in the PLSR co-efficient are related to nucleic acids (794 cm^{-1},1091 cm^{-1}, 1375 cm^{-1}) and proteins (836 cm^{-1} and 1670cm^{-1}). These bands can also be identified on the positive side of PC2 loading which corresponds to spectra of cells analysed 24 hrs post exposure. (table 1).[19,21,23,44] The spectroscopic data, acquired 24 hr after exposure, was also regressed against exposure time, although the correlation co-efficient proved to be almost identical to that of the regression against viability (although inverted) (Figure 3Sb), which is understandable as the viability and time are quite closely (inversely) correlated.

3 | DISCUSSION

Solar radiation is considered one of the principal factors associated with life on earth. A myriad of vital functions carried out by humans, plants and animals are connected with the energy given off by the sun.[49] However, solar radiation is also the most abundant human carcinogen.[50] This mutagenic capacity is mostly attributed to the UV region of the solar spectrum which can be absorbed by DNA and chromophores in the cell.[10,51] This interaction can result in DNA damage, intracellular lipid and protein peroxidation and a dysfunction of the moderating inflammatory and apoptotic cell responses.[5] These events could lead to a final scenario: skin carcinogenesis.[52] The effects of UVR on cells can be seen immediately, and in a delayed manner.[53] The induction of inflammation is one of the most obvious effects on skin.[54] This process occurs in response to an excessive dose of UVR, whereby keratinocyte cells with irreparable UVR damage activate apoptotic pathways and die.[54] Apoptosis is considered to be a regulated and controlled process of cell death.[55] It can be characterised by specific morphological cell patterns, such as nuclear and cytoplasmic condensation and cellular fragmentation into membrane-bound fragments or apoptotic bodies.[56] In this work, the morphological cell analysis after H&E staining reveals, as general features, cell cycle arrest, chromatin condensation and some enlarged cells without complete loss of membrane integrity (Figure 1, column A). These morphological alterations can be associated with the apoptotic pathway as a result of SSR insult,[56,57] and can be more clearly observed in cells 24 hrs post irradiation (Figure 1, column B), including the presence of apoptotic bodies and the loss of contact with their neighbouring cells. The process of progressive cell death can be visualised and quantified using the cytotoxicity assay, AB, as shown in Figure 2. The cell death process induced by SSR can be seen as a monotonic drop in cell viability (Figure 2), indicating that, the longer the exposure the higher the cell damage. Notably, the loss of cell viability is significantly more pronounced 24 hrs after SSR exposure. Ali et

al., and others,[11,58] have also reported a similar decrease in cell viability due to solar radiation in a time dependent manner. To gain further insight into the deleterious effects of SSR in HaCaT cells, Raman spectroscopy was used to characterise and identify biochemical signatures within the nucleus of the cells, immediately after and 24 hrs after irradiation.[11,20,21] Figure 3 presents the average Raman spectrum of a HaCaT cell, highlighting the characteristic bands related to nucleic acids, which confirm the Raman spectra were acquired in the nucleus and not in another subsection of the cell.[59,60] The comparison of the average spectrum of control and irradiated cells (immediately and 24hrs post exposure) respectively do not clearly elucidate DNA damage in cells after irradiation (Figure 1S). Therefore, the multivariate techniques of PCA and PLSR were used to more clearly elucidate changes to the spectral signatures of the biochemical composition of the cells. The spectral variations varied linearly with exposure time and with the measured cell viability response, as measured by AB assay. Figure 4a suggests that only cells irradiated for 180 min analysed immediately after irradiation were clearly differentiated from control cells. The prominence in both the PC2 loading and PLSR co-efficient of bands originating from the DNA backbone moieties at 1093 cm^{-1} and deoxyribose phosphate vibrations at 1121 cm^{-1} and 1460 cm^{-1} suggest possible alterations in the main chain spatial structure of the DNA,[61] while bands located at 792 cm^{-1}, 1375 cm^{-1} and 1657 cm^{-1} indicate that the cells have already embarked upon an apoptotic pathway.[62] The co-efficient of PLSR against exposure time, presents positive features attributed DNA backbone moieties, indicating an increase and/or a conformational change of the biological constituent, while the negative features associated with nucleic acids and deoxyribose indicate direct damage upon exposure time. Each of these features may signify single strand breaks, leading to formation of pyrimidine photoproducts which are associated to replication arrest, as seen in the H&E images, and the formation of reactive oxygen species, which in turn attack the genome.[3,5,7,63] In order to better visualise the biological mechanism response after SSR exposure, spectra recorded from cells immediately after irradiation and 24hrs post exposure were analysed. In both PCA and PLSR analysis, the band centered at 794 cm^{-1}, can be correlated with the progress of nucleosomal DNA cleavage for cells in the late apoptotic phase.[61] Structural changes in the biochemical constituents of lipids and proteins are associated with features of amide I (1670 cm^{-1}), amide III, tyrosine (836 cm^{-1}) and 1438 cm^{-1} (CH2 in lipids/proteins), possibly related to a high concentration of free radicals produced as a primary mechanism of SSR molecular response.[62,64] The presence of the band at 1375 cm^{-1} for cells analysed 24 hrs post exposure indicates progression of nuclear condensation.[61] The amide I signal, previously seen at 1657 cm^{-1} in cells analysed immediately after irradiation, is shifted to 1670 cm^{-1} in cells 24 hrs post exposure, indicating modifications in proteins, and an increased prominence of $\beta - sheet$ as a secondary structure. The results suggest SSR exposure gives rise directly to modifications to the conformational structure of DNA, whereas changes in protein features are mostly seen as a longer term metabolic response to radiation. These results are similar to those reported by Ali et. al.[11], who identified DNA damage occurring at early stages of cytotoxicity and protein modifications related to metabolic changes in cells due to radiation, in reconstructed skin culture models.

It should be noted that the contributions of cell repair mechanisms should also be considered, and could potentially be explored by Raman microespectroscopy. For the case of the effects of the nuclear targeting chemotherapeutic agent doxorubicin, Farhane et al. have attempted to associate differences of in vitro cell-line drug sensitivities with differing levels of activation of anti-apoptotic proteins and DNA repair processes, and identify trends in Raman spectral changes.[65] In a study of the effects of gamma-ray irradiation on HaCaT cells in vitro, Meade et al. explored the manifestations of hyper-radiosensitivity and increased radioresistance at low doses in the dose and time dependent infrared and Raman signatures, and extended the study to analyses of targeted and non-targeted effects of the radiation.[66] Verification of the associated spectral signatures requires correlation with other cytological assay for repair mechanisms (e.g. gamma-H2AX) and anti-apoptotic processes(e.g. BCL-2) and ideally the dose dependence of repair and pro- and anti-apoptotic processes should be systematically mapped out, potentially employing more sophisticated data-mining methods, such as kinetically constrained Multiple Curve Resolution-Alternating Least Squares Regression[67,68]. The potential of Raman microspectroscopy to monitor such effects at a cellular or subcellular level opens up the path to more relevant real life exposures scenarios of repeated doses, of varying duration, and varying periods of intermission.

4 | CONCLUSIONS

This work has illustrated the short term and longer term effects of SSR on the human keratinocyte HaCaT cell line, in vitro, differentiating the cell culture characteristics immediately and 24 hrs post exposure, at a biochemical level. While histological staining can help visualise important changes to cell structure after irradiation, it gives no insight into the direct impact of SSR at a molecular level, where complex biological processes such as photochemical damage are involved or the evolution of the subsequent cellular response. In this context, Raman spectroscopy was demonstrated to have the potential to provide information concerning the biochemical content in

HaCaT cells nuclei, and changes to it, due to SSR exposure. The additional incorporation of multivariate techniques such as PCA and PLSR in parallel with conventional cytotoxicity assays helped to investigate whether differences among spectra of control and irradiated cells were inherently due to cell-to-cell variability or a direct photochemical effect or a metabolic response of cell to SSR.

ACKNOWLEDGMENTS

This study was funded by Consejo Nacional de Ciencia y Tecnología (CONACYT), Mexico.

Author contributions

UL-G performed all experiments, analysis and drafting of the manuscript. AC advised on the experimental protocol. HJB contributed to data analysis and drafting of the manuscript.

Conflict of interest

The authors declare no potential conflict of interests.

SUPPORTING INFORMATION

The following supporting information is available as part of the online article:

Figure S1. Mean Raman spectra of ctrl (i) and 30 min (ii), 60 min (iii), 90 (iv), 120 min (v) and 180 min (vi). Analysed immediately after irradiation (A) and 24 hrs post exposure (B)

Figure S2. Cross-validated MSEP curve for PLSR of Raman spectra of cells analysed immediately after irradiation regressed against exposure time (a) and cells analysed 24 hrs post exposure regressed against cell viability (b). The MSEP have units of minutes (a) and units of cell viability (b).

Figure S3. PLSR modelling of spectroscopic data, acquired immediately after and 24 hrs post exposure regressed against cell viability (a) and time of exposure (b) respectively.

Figure S4. 4S Linear predicted response in PLSR of Raman spectra of cell analysed (a) immediately after irradiation versus time of exposure and (b) 24 hrs post exposure versus cell viability. The solid line depicts the idealised 1:1 correlation.

Figure S5. PCA of Raman spectra of cells analysed (a) immediately after irradiation versus control and b) 24 hrs post exposure vs immediate.

Figure S6. Raw Raman spectra acquired from the nucleus of HaCaT cells irradiated for 30 min, 60 min, 90 min, 120 min and 180 min and analysed immediately and 24 hrs post exposure.

Table S1. Exact contribution for PC1 and PC2, between control and spectra of irradiated cells analysed immediately after irradiation.

Table S2. Exact contribution for PC1 and PC2, between spectra of cells analysed immediately and 24 hrs after irradiation.

References

[1] K. Biniek, K. Levi, R. H. Dauskardt, *PNAS* **2012**, *109* (42), 17111–17116.

[2] A. Modenese, L. Korpinen, F. Gobba, *INT J ENV RES PUB HE* **2018**, *15* (10), 2063.

[3] Yu-Long TANG, Zhou-Yi GUO, *ACTA BIOCH BIOPH SIN* **2005**, *37* (1), 39–46.

[4] J. D'Orazio, S. Jarrett, A. Amaro-Ortiz, T. Scott, *Int. J. Mol. Sci.* **2013**, *14* (6), 12222–12248.

[5] R. M. Brand, P. Wipf, A. Durham, M. W. Epperly, J. S. Greenberger, L. D. Falo Jr, *Frontiers in Pharmacology* **2018**, *9*, 920.

[6] J. Cadet, T. Douki, J. L. Ravanat, *Photochemistry and photobiology* **2015**, *91* (1), 140–155.

[7] R. P. Rastogi, A. Kumar, M. B. Tyagi, R. P. Sinha, *J. Nucleic Acids* **2010**, *2010*.

[8] S. Cho, M. H. Shin, Y. K. Kim, J. E. Seo, Y. M. Lee, C. H. Park, J. H. Chung, in *J INVEST DERM SYMP P*, Elsevier, **2009**, pp. 15–19.

[9] B. H. Mahmoud, E. Ruvolo, C. L. Hexsel, Y. Liu, M. R. Owen, N. Kollias, H. W. Lim, I. H. Hamzavi, *Journal of investigative dermatology* **2010**, *130* (8), 2092–2097.

[10] A.P. Schuch, N.C. Moreno, N.J. Schuch, Menck C.F.M., C.C.M. Garcia, *FREE RADICAL BIO MED* **2017**, *107*, 110–124.

[11] S.M. Ali, F. Bonnier, K. Ptasinski, H. Lambkin, K. Flynn, F.M. Lyng, H.J. Byrne, *Analyst* **2013**, *138* (14), 3946–3956.

[12] P. Karran, R. Brem, *DNA repair* **2016**, *44*, 178–185.

[13] L. A. Compton, G. F. Murphy, C. G. Lian, *Dermatopathology* **2015**, *2* (1), 15–42.

[14] X. Chen, R. J. Swanson, J. F. Kolb, R. Nuccitelli, K. H. Schoenbach, *Melanoma Research* **2009**, *19* (6), 361.

[15] V. Narayanamurthy, P. Padmapriya, A. Noorasafrin, B. Pooja, K. Hema, K. Nithyakalyani, F. Samsuri, *RSC advances* **2018**, *8* (49), 28095–28130.

[16] M. N. Gurcan, L. E. Boucheron, A. Can, A. Madabhushi, N. M. Rajpoot, B. Yener, *IEEE T BIO-MED ENG* **2009**, *2*, 147–171.

[17] H. A. Alturkistani, F. M. Tashkandi, Z. M. Mohammedsaleh, *Glob. J. Health Sci.* **2016**, *8* (3), 72.

[18] N. Kunapareddy, J. P. Freyer, J. R. Mourant, *J. Biomed. Opt* **2008**, *13* (5), 054002.

[19] M. Gargotti, E. Efeoglu, H. J. Byrne, A. Casey, *Anal. Bioanal. Chem.* **2018**, *410* (28), 7537–7550.

[20] D.C. Magdalena, E. Ibrahim, L. P. D. Materon, M. Chipara, *J Nanomed Res* **2016**, *3* (4).

[21] H. J. Byrne, G. D. Sockalingum, N. Stone in *Biomedical Applications of Synchrotron Infrared Microspectroscopy: A Practical Approach*, The Royal Society of Chemistry, **2011**, pp. 105–143.

[22] A.D. Meade, H.J. Byrne, F.M. Lyng, *Mutation Research/Reviews in Mutation Research* **2010**, *704* (1-3), 108–114.

[23] I. Notingher, S. Verrier, H. Romanska, A.E. Bishop, J.M. Polak, L.L. Hench, *Spectroscopy* **2002**, *16* (2), 43–51.

[24] M. Gargotti, U. Lopez-Gonzalez, H.J. Byrne, A. Casey, *Cytotechnology* **2018**, *70* (1), 261–273.

[25] F. Bonnier, A.D. Meade, S. Merzha, P. Knief, K. Bhattacharya, F.M. Lyng, H.J. Byrne, *Analyst* **2010**, *135* (7), 1697–1703.

[26] A. Maguire, F. M. Lyng, J. E. Walsh, *RADIAT PROT DOSIM* **2010**, *140* (2), 147–157.

[27] A. Maguire, B. Morrissey, J. E. Walsh, F. M. Lyng, *INT J RADIAT BIOL* **2011**, *87* (1), 98–111.

[28] J.K.C. Chan, *INT J SURG PATHOL* **2014**, *22* (1), 12–32.

[29] F. Bonnier, M.E. Keating, T.P. Wrobel, K. Majzner, M. Baranska, A. Garcia-Munoz, A Blanco, H.J. Byrne, *Toxicology in vitro* **2015**, *29* (1), 124–131.

[30] Sephra N Rampersad, *Sensors* **2012**, *12* (9), 12347–12360.

[31] M. A. Zachari, P. S. Chondrou, S. E. Pouliliou, A. G. Mitrakas, I. Abatzoglou, C. E. Zois, Michael I Koukourakis, *Dose-Response* **2014**, *12* (2), dose–response.

[32] F. Bonnier, P. Mehmood A.S.and Knief, H. Lambkin, K. Flynn, V. McDonogah, C. Healy, T.C. Lee, F. M. Lyng, H. J. Byrne, *Vibrational Spectroscopy* **2012**, *61*, 124–132.

[33] F. Bonnier, A. Mehmood, P. Knief, A.D. Meade, W. Hornebeck, H. Lambkin, K. Flynn, V. McDonagh, C. Healy, T.C. Lee, *Journal of Raman spectroscopy* **2011**, *42* (5), 888–896.

[34] F. Bonnier, H.J. Byrne, *Analyst* **2012**, *137* (2), 322–332.

[35] Z. Farhane, F. Bonnier, A. Casey, A. Maguire, L. O'Neill, H. J. Byrne, *Analyst* **2015**, *140* (17), 5908–5919.

[36] Z. Farhane, F. Bonnier, A. Casey, H. J. Byrne, *Analyst* **2015**, *140* (12), 4212–4223.

[37] P. Bassan, A. Kohler, H. Martens, J. Lee, H. J. Byrne, P. Dumas, E. Gazi, M. Brown, N. Clarke, P. Gardner, *Analyst* **2010**, *135* (2), 268–277.

[38] L.T. Kerr, B.M. Hennelly, *Chemometrics and Intelligent Laboratory Systems* **2016**, *158*, 61–68.

[39] H. Nawaz, F. Bonnier, P. Knief, O. Howe, F. M. Lyng, A. D. Meade, H. J. Byrne, *Analyst* **2010**, *135* (12), 3070–3076.

[40] Stuart Russell, Peter Norvig, *Artificial Intelligence: A Modern Approach 3rd ed.*, Prentice Hall, NJ, USA, **2009**.

[41] M. Zille, T. D. Farr, I. Przesdzing, J. Müller, C. Sommer, U. Dirnagl, A. Wunder, *Journal of Cerebral Blood Flow & Metabolism* **2012**, *32* (2), 213–231.

[42] N. Kuhar, S. Sil, T. Verma, S. Umapathy, *RSC advances* **2018**, *8* (46), 25888–25908.

[43] Y. Chen, J. Dai, X. Zhou, Y. Liu, W. Zhang, G. Peng, *PLoS One* **2014**, *9* (4), e93906.

[44] A. C. S. Talari, Z. Movasaghi, S. Rehman, *ApSRv* **2015**.

[45] F. Bonnier, P. Knief, B. Lim, A.D. Meade, J. Dorney, K. Bhattacharya, F.M. Lyng, H.J. Byrne, *Analyst* **2010**, *135* (12), 3169–3177.

[46] A. Bruce, A. Johnson, J. Lewis, M. Raff, K. Roberts, P. Walter, *The transport of molecules between the nucleus and the cytosol 4th ed.*, Gerald Sciences, **2002**.

[47] R. WU, G. Ledeen, *Handbook of Neurochemistry and Molecular Neurobiology: Neural Lipids* **2009**, *14*, 173.

[48] M. E. Keating, H. Nawaz, F. Bonnier, H. J. Byrne, *Analyst* **2015**, *140* (7), 2482–2492.

[49] P. K. Mukherjee, *Quality Control and Evaluation of Herbal Drugs: Evaluating Natural Products and Traditional Medicine*, Elsevier, **2019**.

[50] D. A. Brown in *Comprehensive Series in Photosciences*, Elsevier.

[51] A. K. Basu, *Int. J. Mol. Sci.* **2018**, *19* (4), 970.

[52] C. Young, *Occupational medicine* **2009**, *59* (2), 82–88.

[53] R. Wolber, K. Schlenz, K. Wakamatsu, C. Smuda, Y. Nakanishi, V. J. Hearing, S. Ito, *Pigment cell & melanoma research* **2008**, *21* (4), 487–491.

[54] A. Svobodová, J. Vostálová, *Int. J. Radiat. Biol.* **2010**, *86* (12), 999–1030.

[55] C. Krafft, T. Knetschke, R. H.W. Funk, R. Salzer, *Analytical chemistry* **2006**, *78* (13), 4424–4429.

[56] S. L. Fink, B. T. Cookson, *Infection and immunity* **2005**, *73* (4), 1907–1916.

[57] Q. Chen, J. Kang, C. Fu, *Signal transduction and targeted therapy* **2018**, *3* (1), 1–11.

[58] R. Masuma, M. Kashima, T. Okuno, *J Photochem Photobiol B.* **2013**, *125*, 202–208.

[59] L. Jianghua, D. Yong, Z. Musheng, *Journal of NasoPharyngeal Carcinoma* **2014**, *1* (17).

[60] K. Okotrub, N.V. Surovtsev, V.F. Semeshin, L.V. Omelyanchuk, *Cytometry Part A* **2015**, *87* (1), 68–73.

[61] E. Brauchle, S. Thude, S. Y. Brucker, K. Schenke-Layland, *Sci. Rep* **2014**, *4* (1), 1–9.

[62] S.P. Singh, S. Kang, J. W. Kang, P.T.C. So, R. R. Dasari, Z. Yaqoob, I. Barman, *Scientific reports* **2017**, *7* (1), 1–8.

[63] Y. Matsumura, H. N. Ananthaswamy, *TOXICOL APPL PHARM* **2004**, *195* (3), 298–308.

[64] B. Poljšak, R. Dahmane, *Dermatology research and practice* **2012**, *2012*.

[65] Z. Farhane, F. Bonnier, M. A. Maher, J. Bryant, A. Casey, H. J. Byrne, *Journal of biophotonics* **2017**, *10* (1), 151–165.

[66] A. D. Meade, O. Howe, V. Unterreiner, G. D. Sockalingum, H. J. Byrne, F. M. Lyng, *Faraday discussions* **2016**, *187*, 213–234.

[67] D. Perez-Guaita, G. Quintas, Z. Farhane, R. Tauler, H. J. Byrne, *Talanta* **2019**, *208*, 120386–120386.

[68] D. Perez-Guaita, K. Chrabaszcz, K. Malek, H. J. Byrne, *Journal of Biophotonics* **2020**.

GRAPHICAL ABSTRACT TEXT

This work monitors the impact of solar radiation at a molecular level in keratinocytes by Raman spectroscopy

GRAPHICAL ABSTRACT FIGURE

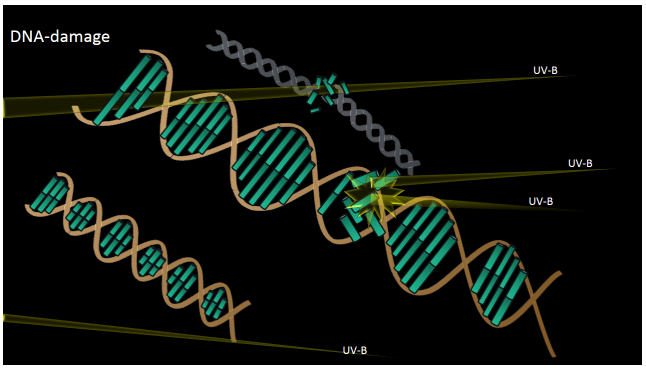

How to cite this article: Lopez-Gonzalez U., A. Casey, and H.J. Byrne (2020), Monitoring the biochemical changes ocurring to human keratinocytes exposed to solar radiation by Raman spectroscopy, *J. Biophotonics*, .